Hydrodynamics of ciliary propulsion

Antoine Dauptain, Julien Favier, Alessandro Bottaro

Hydrodynamics of ciliary propulsion

A. Dauptain, J. Favier, A. Bottaro

DICAT, Università di Genova, Via Montallegro 1, 16145 Genova, Italy

Abstract

A numerical approach is developed to study the effect on a fluid of the regular oscillations of an array of flexible cilia which hinge around points on a wall. The specific application studied concerns the ctenophore *Pleurobrachia pileus*, a small marine invertebrate of quasi-spherical shape and diameter of the order of the centimeter which swims in water thanks to the rhythmic beating of eight rows of hair-like cilia aligned along its body. Only one row of cilia is studied here, in a three-dimensional setting. The technique presented is general enough to allow its application to a variety of fluid-structure interaction problems. The physical mechanisms of the propulsion are highlighted, by analysing the results of three-dimensional simulations. A parametric study involving *natural* and *non-natural* parameters leads to a better understanding of the propulsive characteristics of ctenophores; results show that the specific power expended increases with the increase of the beating frequency of the row of cilia, in agreement with experiments.

1. Introduction

1.1. General scope

Cilia and flagella are little-noticed but pervasive features of animals and plants, accomplishing - through their movement or simply through their presence - a large variety of tasks (Lodish et al., 2000). Motile cilia are whip-like appendages extending from the surface of many types of cells, and designed to move either the cell itself or the fluid around it. Their behavior is a consequence of their complex internal structure, which is essentially the same in both eukaryotic flagella and cilia, and is based on the interaction of a set of microtubules. These can bend under the action of dynein arms, powered by ATP, thus generating typical oscillations. Progress in the computational modelling of the internal axoneme of a flagellum has been recently reviewed by Fauci and Dillon (2006). From the "external" point of view, the major differences between motile cilia and flagella can be seen *(i)* in their length, *(ii)* in the fact that cilia appear in densily packed arrays, whereas flagella act mostly individually or in couples, and *(iii)* in the characteristics of their beating which determines the direction of the induced thrust.

Though this paper will be devoted to a very specific kind of ciliary motion, it is not useless to briefly outline a few of the functions played by such organelles, to provide an idea of their usefulness and broad range of applications:

- a single flagellum is used by sperm cells to move forward;
- in all female mammals, the beating of cilia in the Fallopian tubes moves the ovum from the ovary to the uterus;
- about 80% of the epithelial cells in the human trachea are ciliated. Cilia sweep mucus and trapped particles into the throat where they are usually swallowed and expelled;
- the cochlea in the inner ear is lined with cilia, which oscillate after sensing vibrations transferred from the middle ear thus triggering the generation of nerve impulses, conveyed to the brain as bursts of acoustic information;

- the asymmetric motion of embryonic fluid produced by beating cilia affects the expression of genes located on the left hand side of the embryo of many vertebrates. The same genes remain inactive on the right hand side of the body, thus apparently determining inner organ placement and the left-right asymmetry in the body axis (Tabin, 2006);
- ciliary defects can lead to several human diseases (Gardiner, 2005).

The interaction between cilia and flagella with their environment has attracted in the last half century the interest of physicists and engineers, motivated also by the possible use of cilia-based actuators as micro-mixers, for flow control in tiny biosensors, or as micropumps for drug-delivery systems.

The study of the hydrodynamics of a beating flagellum was initiated in 1951 by G.I. Taylor, who analyzed the locomotion induced on a body by a tail beating in a regular manner, and found an approximate relation linking the velocity of the organism to the propagation speed of the tail wave. Other studies followed in which many cilia, covering flat or curved surfaces and oscillating synchronously, were considered and for which local models of the hydrodynamic interaction between cilia and the surrounding fluid were needed. These research activities were initiated with the observation that organisms appear to benefit from adjusting the phase relationship of the beat patterns of neighboring cilia, and that metachronal waves are common in the oscillations of cilia and flagella. The early activity is comprehensively reviewed by Brennen and Winet (1977), and is mostly focussed on isolating and understanding aspects of the self-propelling behavior. To simplify things, inertial effects were neglected, because of the small dimensions and low velocities at play. The more or less densely packed arrays of cilia were treated by local interaction models which, despite the approximations made, were quite successful at reproducing features of the motion. They can be grouped into two categories: the *envelope* model (Taylor, 1951; Reynolds, 1965; Tuck, 1968; Blake, 1971b,a; Brennen, 1974) and the *sublayer* model (Blake, 1971b,a; Keller et al., 1975; Lighthill, 1976; Phan-Thien et al., 1987). In the envelope model the cilia are assumed to be closely packed together so that the fluid effectively sees a waving material surface enveloping the top of the layer. The principal limitations of this approach lie in the small amplitude approximation for the oscillations of the material surface and in the impermeability and no-slip condition imposed at the envelope sheet. The sublayer approach is not limited to small amplitudes, and models the distribution of Stokes flow force singularities along each cilium with an equivalent body force. The key assumption here is in how the interaction among individual cilia is modelled: in the formulation by Blake (1971b) such an interaction force is steady, whereas Keller et al. (1975) improved the model by including unsteadiness. Both the envelope and the sublayer approach yield results in qualitative agreement with observations in their respective ranges of applicability. Clearly the details of the hydrodynamics within the cilia array and the effect of possibly non-negligible inertial terms posed problems which, until recently, were overwhelming.

In more recent times, advances in experimental techniques have rendered the problem amenable to laboratory investigation and some papers appeared which questioned the hydrodynamic results of the proposed models (Matsumoto, 1991; Barlow et al., 1993). Progress in computational fluid dynamics and in the available hardware make the problem tractable also by a numerical approach.

1.2. Configuration studied

To fix things we have considered a very specific case, the locomotion characteristics of the ctenophore *Pleurobrachia pileus* (commonly known as the "sea gooseberry") which, as we will see below, is outside the range of approximation of former models. In such a small organism (*cf.* Figure 1) the thickness of the layer of cilia is much smaller than the body characteristic dimension, so that it is acceptable to consider a flat layer of cilia exhibiting planar beat patterns. Propulsion is produced by the oscillations, at a particular frequency, of eight rows of cilia, disposed around the body and aligned with it, each one of which is composed by hundred thousands or more cilia. The beating pattern exhibits an antiplectic metachronism, *i.e.* each individual cilium presents a definite phase relationship with its neighbours, and the wave propagates in a direction opposite to the effective stroke.

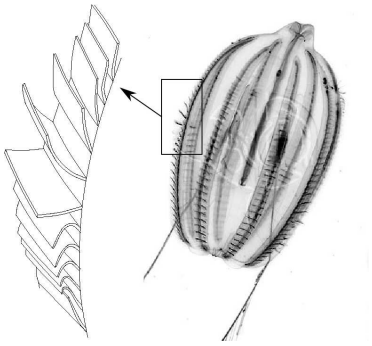

Fig. 1. Propulsive row of cilia on a *Pleurobrachia*.

Figure 2(a) shows the positions occupied by a cilium within one beating period. During the effective stroke (towards the left) the cilium is straight and a high velocity region is created behind the cilium, near its tip. In the recovery phase the high-velocity patch is released towards the left, while the cilium bends and moves to the right. This kind of behavior lies at the heart of the propulsive efficiency of the *Pleurobrachia*.

Considering an array of cilia of the *Pleurobrachia*, when metachronal strokes are brought towards the left, a right-propagating wave is produced and the body is propelled to the right (*cf.* Figure 2(b)). The aim of this paper is to focus on this propulsive mechanism, by looking at the action of a row of cilia on the surrounding fluid; different beating parameters will be tested to assess their effect on the power output.

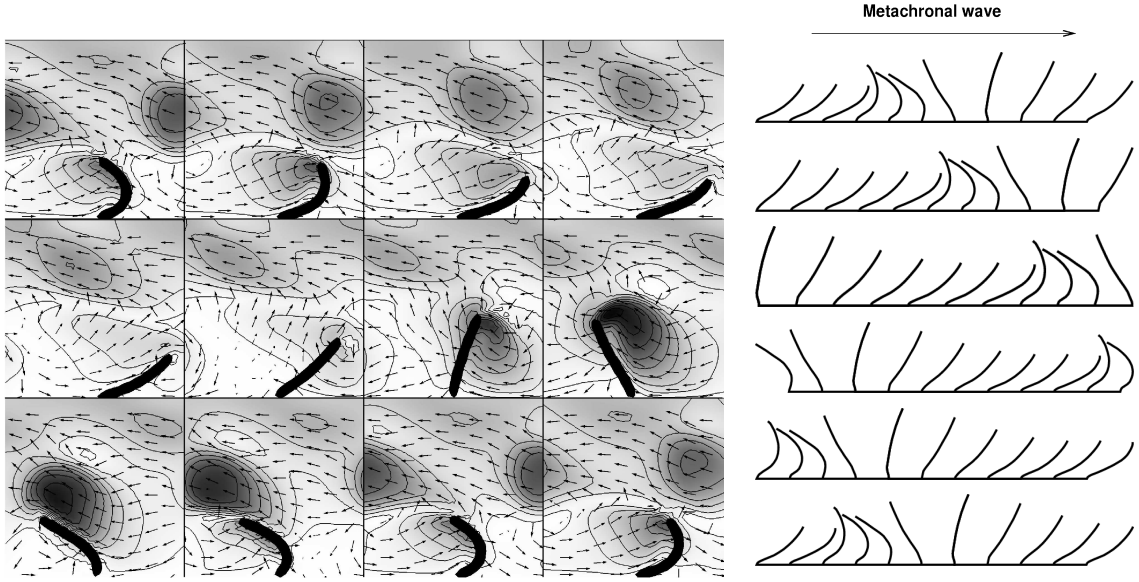

(a) Motion of a single cilium starting from rest. (b) One antiplectic period.

Fig. 2. Beating pattern on a *Pleurobrachia*. (a) Successive images of a beating cilium in a periodic domain, equally spaced within a period in time, must be seen as in a comic strip. In the symmetry plane of a three-dimensional simulation (*cf.* §2.), the velocity amplitude is represented with grey-scale contours with spacing of 20 mm/s; the velocity direction is given by constant-length arrows. (b) One wave of beating cilia observed on a real *Pleurobrachia*. Time increases from top to bottom; the organism is propelled towards the right, in the same direction as the metachronal wave.

2. Numerical procedure

Cilia position and velocity are digitized from stroboscopic recording of the movement of a real *Pleurobrachia* performed by Barlow et al. (1993) and Barlow and Sleigh (1993). These data are then imposed in the fluid solver by using an immersed boundary method (IBM) (Fadlun et al., 2000; Peskin, 2002; Mittal and Iaccarino, 2005; Zhang and Gay, 2007).

The Reynolds number, based on tip speed of the cilium, its length L and the kinematic viscosity of water, ranges from 50 to 200; since the Stokes approximation is not tenable, a Navier-Stokes code is used to solve the incompressible laminar flow problem in three dimensions. The technique employs a staggered grid with a second order scheme in space and time, based on a classical predictor-corrector method for the pressure coupling (Yang et al., 2008).

The numerical resolution of this one-way-coupling problem (with the structures, *i.e.* the cilia, forcing the fluid) is performed by decomposing the main problem into three subproblems (extraction of position and velocity of cilia, IBM, fluid problem) that are controlled by a coupler, PALM (Buis et al., 2005), to ensure a straightforward development towards more general applications for fluid-structure interaction problems. We use this partitioned approach in order to have good control on each component of the process, independently from the others. The PALM software allows easy manipulation of global objects (fluid solver, structure solver, post-processing, etc.) and their mutual interaction via a graphical user-friendly interface. Another advantage of PALM is that any of the constitutive elements of the system (the fluid solver for example) can be easily replaced without modifying the global framework. PALM is conceived so that the communications between individual modules are handled by a convenient and optimized memory buffer management.

The accuracy of imposing a prescribed time-dependent velocity field within the continuum has been tested for a few different implementations of the IBM in Dauptain et al. (2007), where different impositions of immersed boundary conditions are compared. To match the cilium velocity distribution $\mathbf{V}$ to that on the boundary S of the cilium, a volume force field $\mathbf{f}$ is introduced in the computational domain. The incompressible Navier-Stokes and continuity equations are

$$\frac{\partial \mathbf{u}}{\partial t} + (\mathbf{u} \cdot \nabla)\mathbf{u} = -\frac{1}{\rho}\nabla p + \nu \nabla^2 \mathbf{u} + \mathbf{f}\,;\, \nabla \cdot \mathbf{u} = 0.$$

In this study we use the *feedback forcing technique* (Peskin, 2002) in which the volume force $\mathbf{f}$, for a solid boundary located in $\mathbf{x}_s$ at time t and moving at speed $\mathbf{V}$, is defined as

$$\mathbf{f}(\mathbf{x}_s, t) = \alpha_f \int_0^t \left[\mathbf{u}(\mathbf{x}_s, t) - \mathbf{V}(\mathbf{x}_s, t)\right] dt' + \beta_f \left[\mathbf{u}(\mathbf{x}_s, t) - \mathbf{V}(\mathbf{x}_s, t)\right].$$

In this expression α_f and β_f are negative constants, heuristically determined so that a measure of the difference $\mathbf{u}(\mathbf{x}_s, t) - \mathbf{V}(\mathbf{x}_s, t)$ is minimized. The time-dependent feedback is neglected ($\alpha_f = 0$) because the needed volume force varies much in amplitude and direction; the optimal intantaneous feedback is found for $|\beta_f| \simeq 6400$ s^{-1} in a typical simulation. For larger $|\beta_f|$ the volume force displays spurious oscillations.

A second crucial step in the IBM is the interpolation strategy. This is even more delicate in the present setting, because of the rapidly moving boundary, and the small dimensions of the moving bodies. Indeed, the position of each cilium is specified in the continuum and in the feedback forcing technique the volume force $\mathbf{f}(\mathbf{x}_s, t)$ must be distributed among the grid points surrounding the bodies in motion. A comparison with other approaches is presented by Dauptain et al. (2007).

We start by observing that on the two-dimensional beating plane each cilium is made up by M points, and moves in a computational domain containing about N^2 cells, with $M > N$ (for example M=40 and N=16). For each of the M points within a cilium $\mathbf{x}_s$, the closest cells $\mathbf{X}_{i,j}$ in the grid are searched for. The indices i and j indicate, respectively, the discretization nodes along the wall-parallel direction, x, and the wall-normal direction, y; the corresponding velocity components are called u and v. The properties of the cilium are spread among the 24 grid points $\mathbf{X}_{i,j}$ by multiplying the discrete forcing function by a filter function $h(i, j; \mathbf{x}_s)$ (*cf.* Figure 3 where all the grid points in the discretization stencil are represented with open circles.). When a grid point $\mathbf{X}_{i,j}$ is influenced by more than one $\mathbf{x}_s$ an averaging procedure is performed. The chosen filter function in two dimensions is:

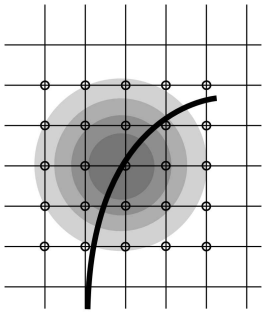

Fig. 3. Interpolation strategy.

$$h(i, j; \mathbf{x}_s) = \frac{1 - \tanh\left(\frac{r-1}{0.5}\right)}{2}\,;\, r = \sqrt{\left(\frac{x_s - X_{i,j}}{\Delta x}\right)^2 + \left(\frac{y_s - Y_{i,j}}{\Delta y}\right)^2}.$$

The volume force $\mathbf{f}(\mathbf{x}_s, t)$ is then applied to all the points in the discretization stencil and is zero elsewhere. The large variations in the amplitude of the velocity and in the direction of the different segments which compose a cilium - and the way the exact movement of the body is discretized in the available grid - can be represented in several manners; we have chosen to display them plotting the u-velocity component against the v-component of different points on the cilium in the course of time.

Figure 4 illustrates the prediction obtained for the realistic beating of the single flexible cilium, such as that in Figure 2(a). From the hodograph plane representation it appears that the largest errors with respect to the target velocity occur approximately halfway through the effective stroke phase of the cilium, when the horizontal velocity attains its minimum value. The maximum errors in velocity amplitude, less than 6%, are due to the interpolation procedure and occur at the cilium tip and at $\frac{1}{4}L$, during strong acceleration and deceleration phases.

We consider this method sufficiently accurate to analyze the flow field around bodies moving at relatively high frequencies within a fluid; we thus proceed with a parametric study of the motion of arrays of cilia executing an antiplectic metachronal wave, with the goal of identifying efficient beating parameters.

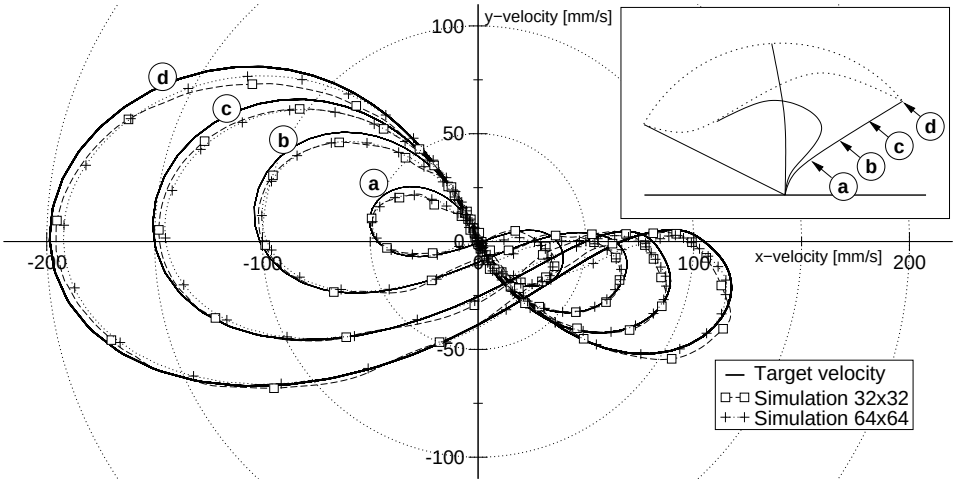

Fig. 4. Velocity at different points within a realistically beating cilium.

3. Results

3.1. Flow topology

A snapshot of the flow is shown in Figure 5 for the case of 8 cilia beating at 10 Hz, displaying color contours of the velocity amplitude in a plane of symmetry, together with gray scale contours of the relative pressure field $P - P_{\text{ref}}$ on the ground plane (P_{ref} is the reference pressure at $(x,y,z)=(0,4L,2L)$, with x the streamwise direction, y the normal-to-the-wall direction and z the spanwise direction).

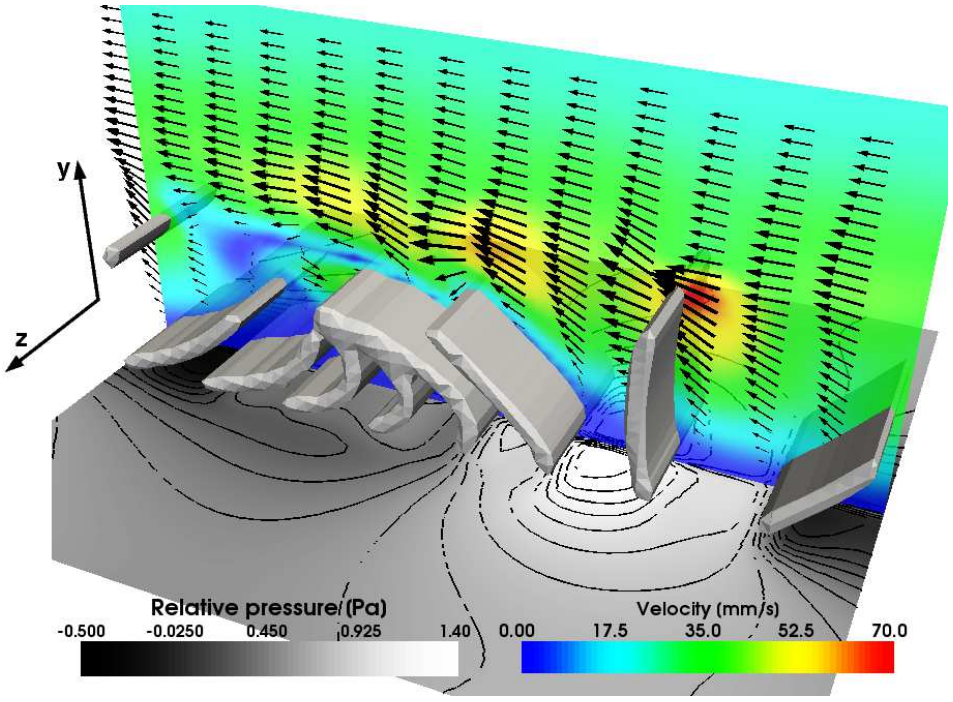

Fig. 5. Three-dimensional result for $n = 8$ cilia and $f = 10$ Hz. Cilia are beating towards the left and the metachronal wave goes toward the right (antiplectic motion). Black arrows represent the velocity vectors. Pressure contours on the horizontal plane are spaced 0.1 Pa apart. The cilia are represented by isosurfaces of the distribution function of the volume force used in the immersed boundary method.

The computational box in the spanwise and normal directions runs from $z = 0$ (the cilia are cut into two, and a symmetry condition is enforced) to $z = 2L$ (L is the characteristic cilium length, taken here equal to 1 mm). Along y the domain runs from $y = 0$ to $y = 4L$. The boundary conditions of the $64 \times 64 \times 32$ computational cartesian grid are: periodic for inflow and outflow along x, no-slip bottom wall and slip top wall, plus symmetry conditions on the sides.

In the velocity field in Figure 5, three high-velocity regions are visible close to $y = L$. The high-speed patch on the right hand side is generated by a paddling effect at the tip of the corresponding cilium, during the maximum acceleration of the stroke phase. The neighboring patches, more to the left, are fed by a blowing effect which takes place when the cilia move close to one another. The pressure field shows low and high pressure regions, corresponding respectively to the beginning (aspiration effect) and the end (blowing effect) of the effective stroke phase.

For this same case, a comparison is possible with PIV data (Barlow and Sleigh, 1993) in the symmetry plane ($z = 0$) of the ctene rows. Figure 6 attests to a satisfactory agreement; for instance, the positions of four identifiable high-speed patches (noted from A to D in the Figure), correspond roughly to the measured ones. The velocity peak in zone A is underestimated by the simulations (about 25 mm/s instead of 35 mm/s). Conversely, regions B, C and D are overestimated by close to 10 mm/s. It is possible that these discrepancies are attenuated when proper account is given to the curvature of the body.

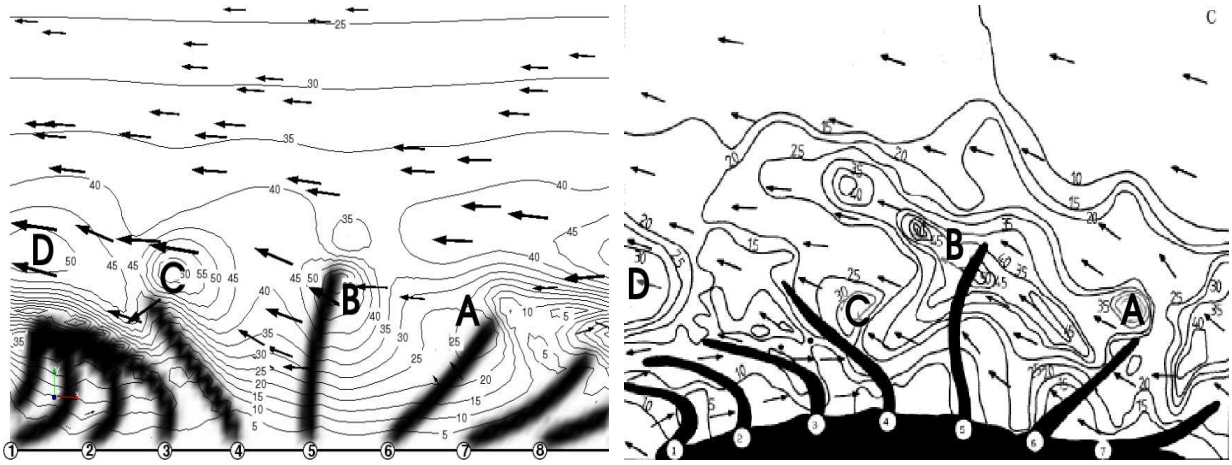

(a) Present numerical simulations. (b) Experiments (Barlow and Sleigh, 1993).

Fig. 6. Comparison of a simulated flow field with an experimental micro-PIV velocity field. The contours show the speed of water in mm/s and the arrows show the direction of the velocity field. The physical size of the image is about 3 mm × 2 mm.

3.2. Velocity fields

The wavelength λ of the metachronal wave is always linked to the number of cilia n present through the relation: $\lambda = nL/2$, *i.e.* the spacing between any two neighboring cilia along the wall is generally fixed at $L/2$, which corresponds to the normal spacing for the *Pleurobrachia*. The mean streamwise velocity profile is given in Figure 7(a), showing a boundary layer-like profile lifted from the wall by $L/2$, in qualitative agreement with analytical results by Keller et al. (1975).

Figure 7(b) shows the $|u|$ and v phase-averaged velocity profiles at $y = L$ as function of x/λ. The interval $0 < x/\lambda < 0.7$ corresponds to the stroke phase, and $0.7 < x/\lambda < 1$ to the recovery phase. Inside the stroke phase, aspiration, paddling and blowing effects are located respectively at $[0, 0.25]$, $[0.25, 0.35]$ and $[0.35, 0.7]$. Indeed, $|u|$ and v display simultaneously their maximum values during the paddling phase, the minimum of $|u|$ occurs during the recovery phase, and v becomes negative during the aspiration phase.

The fact that v shows positive and negative values over one period, suggests a blowing and suction-like behavior through a fictitious wall; this indicates that the assumptions inherent to the analytical envelope model (Blake, 1971a; Brennen, 1974) would be poorly satisfied in this case.

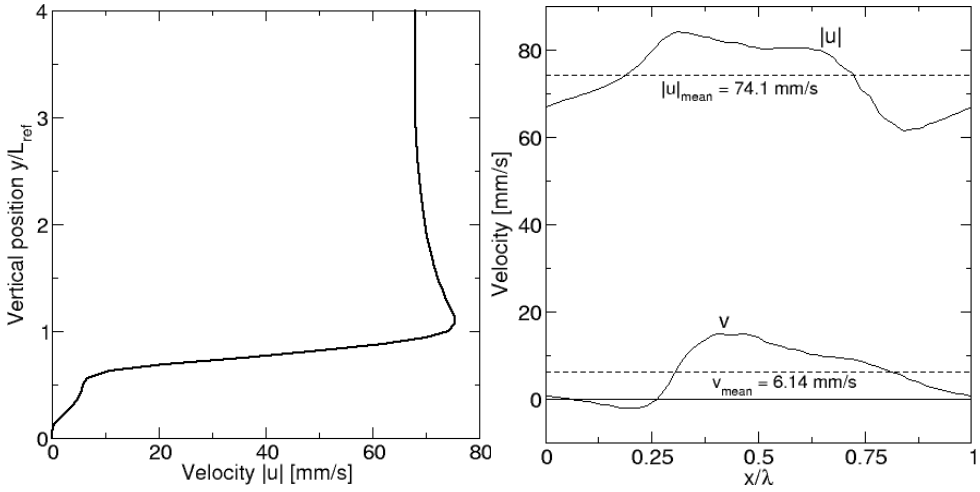

(a) Vertical mean profile at $z = 0$. (b) Longitudinal profile at $y = L$ and $z = 0$.

Fig. 7. Velocity profiles on the symmetry plane ($z = 0$, *i.e.* in the mid-plane of each cilium) for $f = 15$ Hz and $n = 12$ cilia. (a) Velocity profile averaged over time and streamwise direction $\mathbf{x}$. (b) Phase-averaged velocity over time and along a wavelength.

Integrating along x for $y = L$, a positive average v_{mean} of 6.14 mm/s is found. This output of fluid from the top row of cilia implies an influx of fluid through the sides. Hence, three-dimensional suction occurs mainly on the sides of the cilia, while blowing essentially takes place through the top surface. The phase-averaged value of the longitudinal velocity u_{mean} at $y = L$ is 74.1 mm/s, so that the field is dominated by a streamwise-oriented motion.

3.3. Energy budget

It is simple to derive the energy equation, and to find the terms which contribute the most to an increase of the kinetic energy of the flow. By taking the integral over a volume V (limited in y between 0 and L and running through a wavelength in x) of the scalar product of the Navier-Stokes equations with $\mathbf{u}$, it is easy to find

$$\frac{d}{dt}\int_V (\frac{1}{2}\mathbf{u}.\mathbf{u})\, dV = P + D + S,$$

where P is a production term, D is a negative-definite dissipation term, and S is a source term related to the presence of a volume force $\mathbf{f}$, with

$$P = \int_V (-u\, v)\, (u_y + v_x)\, dV,$$

$$D = -\nu \int_V \left[(u_x)^2 + (v_x)^2 + (u_y)^2 + (v_y)^2\right]\, dV,$$

$$S = \int_V \mathbf{u}.\mathbf{f}\, dV,$$

and subscripts denote partial derivatives. It is found that in all cases considered, the source term, linked to the beating power expended by the *Pleurobrachia* to move in water, is completely balanced by the action of viscosity. The propulsive performances of the *Pleurobrachia* are related to the blowing/suction effect previously described and are direct functions of the beating parameters. A study is thus called for to identify optimal parameters and to verify whether they match the swimming characteristics of the animal. The ability to associate the beating parameters to specific physical events is a prerequisite to the conception and realization of a technology capable of exploiting well-defined flow features and mimicking the motion of the *Pleurobrachia*.

3.4. *Parametric study and discussion*

Barlow and Sleigh (1993) observed that the *Pleurobrachia* uses a combination of beating frequency and number of cilia per wave specific for each speed: 5 Hz and 25 cilia for low speed, 15 Hz and 12 cilia for cruise speed, 25 Hz and 9 cilia for escape/hunting speed (short bursts).

To understand this natural optimization process, the propulsive performances of ctenophores are studied, the frequency varying from 5 Hz to 25 Hz and the number of cilia in a wavelength varying from 9 to 25. In Table 1 the performances *per cilium* are reported and the sets of parameters corresponding to *natural performances* are highlighted in bold. The power output is defined by the energy transfer from the organelle to the flow, and the propulsive velocity U by the longitudinal fluid speed observed far from the body surface. The velocity U is normalized by the largest longitudinal velocity at the tip of the cilium U_{tip}. On the right side of Table 1, the parameter R, defined as the ratio of propulsive velocity to the power output per cilium, is reported.

Table 1. Comparative influence of beating parameters, number of cilia n and frequency f, on the performances (power output, velocity ratio U/U_{tip} and performances index R).

Power output [nW/cilium]				U/U_{tip}				$R = U/P_{p.c.} \times 100$ [m s^{-1} nW^{-1}]			
	$n = 9$	$n = 12$	$n = 25$		$n = 9$	$n = 12$	$n = 25$		$n = 9$	$n = 12$	$n = 25$
f=5 Hz	1.83	1.69	**1.51**	f=5 Hz	0.35	0.32	**0.25**	f=5 Hz	0.69	0.67	**0.83**
f=15 Hz	39.3	**36**	32.7	f=15 Hz	0.69	**0.65**	0.65	f=15 Hz	0.19	**0.21**	0.23
f=25 Hz	**144**	136	128	f=25 Hz	**0.78**	0.76	0.76	f=25 Hz	**0.10**	0.12	0.12

The power output strongly increases with the frequency and decreases slowly with the number of cilia ($P \sim f^{2.5} n^{-0.3}$), and so does the velocity ratio ($U/U_{\text{tip}} \sim f^{1.13} n^{-0.25}$). As expected, large values of the power output are found in the case of long waves and high beating frequencies. Such conditions are however very demanding on the side of the animal. They could only be produced in very short bursts, if at all. The ratio R of propulsive speed to expended power is not maximized by the natural beating parameters of the *Pleurobrachia*, indicating that such a simple functional is not sufficient to capture all the features involved in the propulsion of ctenophores.

The results are then compared to those obtained experimentally by Barlow and Sleigh (1993), although the latter authors approximate the power output in a crude manner, mainly because of the difficulty to gather experimental data on a real *Pleurobrachia*. The observed trends are in rough agreement (*cf.* Figure 8). We emphasize the fact that three-dimensional simulations are necessary in this case to model correctly this flow configuration. Indeed in the two-dimensional case which was tested previously (Dauptain et al., 2007), an overestimation of the power output was observed, compared to experimental data, mainly linked to the blowing effect which was larger than expected. A more realistic three-dimensional simulation allows fluid to escape from the sides of cilia, while in the two-dimensional case the fluid can only be ejected via the top surface.

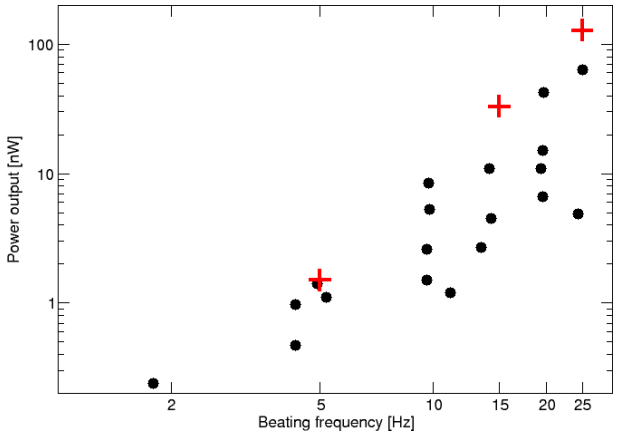

Fig. 8. Comparison of power outputs *per cilium* as function of the beating frequency. Dots: experiments by Barlow and Sleigh (1993); crosses: present numerical results for the *natural* beating cases.

Another feature which is interesting to examine, while maintaining the beating motion unaltered, is the variation in the spacing between neighboring cilia. We have thus considered the case of a wave of period 6 L (*i.e.* $\lambda = 6$ mm), for a varying number of beating cilia within the wavelength, at the fixed frequency of 15 Hz. The effect of cilia interspace Δx, normalized by L, is reported in Figure 9(a). A maximum of R is encountered for $\Delta x/L = 0.5$ (which is the natural spacing of the cilia) while the velocity ratio decreases linearly and slowly when the cilia interspace $\Delta x/L$ increases towards 1 (Figure 9(b)).

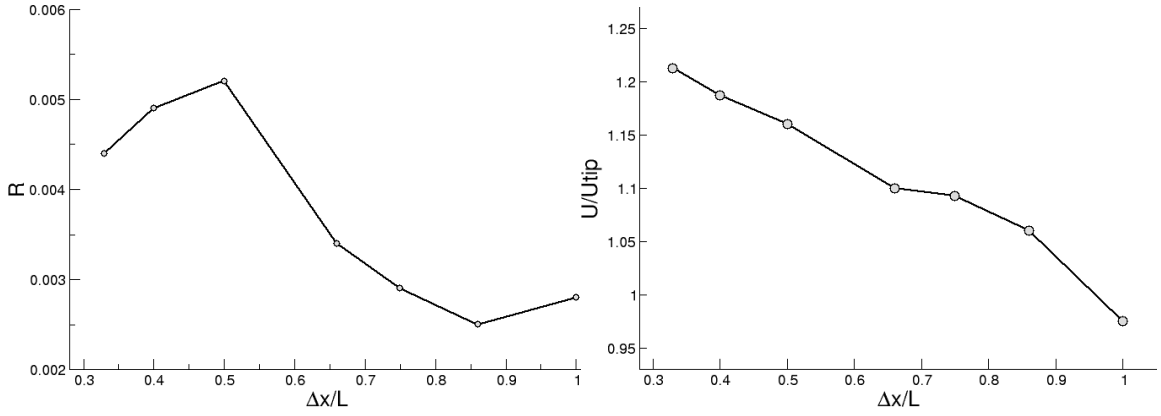

(a) $R = \dfrac{U}{P_{p.c.}}$. (b) Velocity ratio U/U_{tip}.

Fig. 9. Effect of *non-natural* spacing among neighboring cilia. The results refer to two-dimensional simulations, but few calculations carried out in three dimensions support the trends in the figures.

4. Concluding remarks

The numerical procedure developed, based on the use of a coupling software (PALM) and an immersed boundary procedure, is efficient and capable to model the influence of a flexible beating structure on the near-wall surrounding fluid. The specific application considered focuses on the propulsive characteristics of a small ctenophore: it is shown that beating patterns constituted by long waves oscillating at high frequencies yield very large propulsive velocities (a mechanism possibly exploited by the *Pleurobrachia* when in need of short bursts), and that the power output per cilium increases with the frequency as $f^{2.5}$ during swim at natural conditions, in rough agreement with laboratory data. During its normal swimming phases, the animal does not simply maximize the ratio of longitudinal propulsion velocity to power expended. Perspectives concern the two-way interaction between freely beating cilia and the fluid (Yang et al., 2008).

Acknowledgement

The authors acknowledge the support of the EU through the Marie Curie EST program Flubio, contract number 20228-2006.

References

Barlow, D., Sleigh, M., 1993. Water propulsion speeds and power output by comb plates of the Ctenophore *Pleurobrachia pileus* under different conditions. Journal of Experimental Biology 183, 149–163.

Barlow, D., Sleigh, M., White, R., 1993. Water flows around the comb plates of the Ctenophore *Pleurobrachia* plotted by computer: a model system for studying propulsion by antiplectic metachronism. Journal of Experimental Biology 177, 113–128.

Blake, J., 1971a. Infinite models for ciliary propulsion. Journal of Fluid Mechanics 49, 209–222.

Blake, J., 1971b. A spherical envelope approach to ciliary propulsion. Journal of Fluid Mechanics 46, 199–208.

Brennen, C., 1974. An oscillating-boundary-layer theory for ciliary propulsion. Journal of Fluid Mechanics 65, 799–824.
Brennen, C., Winet, H., 1977. Fluid mechanics of propulsion by cilia and flagella. Annual Review of Fluid Mechanics 9, 339–398.
Buis, S., Piacentini, A., Déclat, D., 2005. PALM: a computational framework for assembling high-performance computing applications. Concurrency and Computation: Practice and Experience 18 (2), 231–245.
Dauptain, A., Favier, J., Bottaro, A., June 18-22, 2007. Hydrodynamics of beating cilia. In: Springer (Ed.), Proceedings of IUTAM Symposium on Unsteady Separated Flows and their Control. Corfu, Greece.
Fadlun, E. A., Verzicco, R., P., O., Mohd-Yusof, J., 2000. Combined immersed-boundary finite difference methods for three-dimensional complex flow simulations. Journal of Computational Physics 161, 35–60.
Fauci, L., Dillon, R., 2006. Biofluidmechanics of reproduction. Annual Review of Fluid Mechanics 38, 371–394.
Gardiner, M., 2005. The importance of being cilia. Howard Hughes Medical Institute Bulletin 18 (64), 33–36.
Keller, S., Wu, T., Brennen, C., July 8-12 1974 1975. A traction layer model for ciliary propulsion. In: Plenum Press, New York. Pasadena, Ca., pp. 253–271.
Lighthill, J., 1976. Flagellar hydrodynamics. SIAM Review 18, 161–230.
Lodish, H., Berk, A., Zipursky, L., Matsudaira, P., Baltimore, D., Darnell, J., 2000. Molecular Cell Biology. Fourth Edition. W.H. Freeman and Co., New York, NY.
Matsumoto, G., 1991. Swimming movements of Ctenophores, and the mechanics of propulsion by ctene rows. Hydrobiologia 216-217, 319–325.
Mittal, R., Iaccarino, G., 2005. Immersed boundary methods. Annual Review of Fluid Mechanics 37, 239–261.
Peskin, C. S., 2002. The immersed boundary method. Acta Numerica 11, 479–517.
Phan-Thien, N., Tran-Cong, T., Ramia, M., 1987. A boundary element analysis of flagellar propulsion. Journal of Fluid Mechanics 184, 533–549.
Reynolds, A., 1965. The swimming of minute organisms. Journal of Fluid Mechanics 23, 241–260.
Tabin, C., 2006. The key to left-right asymmetry. Cell 127, 27–32.
Taylor, G. I., 1951. Analysis of the swimming of microscopic organisms. Proceedings of the Royal Society A209, 447–461.
Tuck, E., 1968. A note on a swimming problem. Journal of Fluid Mechanics 31, 305–308.
Yang, J., Preidikman, S., Balaras, E., 2008. A strongly coupled, embedded-boundary method for fluid-structure interactions of elastically mounted rigid bodies. Journal of Fluids and Structures 24, 167–182.
Zhang, L., Gay, M., 2007. Immersed finite element method for fluid-structure interactions. Journal of Fluids and Structures 23, 839–857.